NANO LETTERS

pubs.acs.org/NanoLett

Letter

Optical Pulling Forces Enabled by Hyperbolic Metamaterials

Renchao Jin, Yihao Xu, Zheng-Gao Dong,* and Yongmin Liu*

Cite This: *Nano Lett.* 2021, 21, 10431−10437

Read Online

ACCESS | Metrics & More | Article Recommendations | Supporting Information

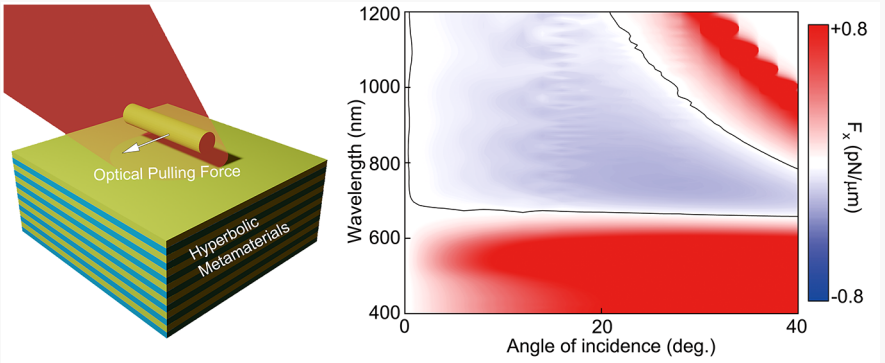

ABSTRACT: We propose a novel approach to generating optical pulling forces on a gold nanowire, which are placed inside or above a hyperbolic metamaterial and subjected to plane wave illumination. Two mechanisms are found to induce the optical pulling force, including the concave isofrequency contour of the hyperbolic metamaterial and the excitation of directional surface plasmon polaritons. We systematically study the optical forces under various conditions, including the wavelength, the angle of incidence of light, and the nanowire radius. It is shown that the optical pulling force enabled by hyperbolic metamaterials is broadband and insensitive to the angle of incidence. The mechanisms and results reported here open a new avenue to manipulating nanoscale objects.

KEYWORDS: *optical pulling force, hyperbolic metamaterial, plasmonics, gold nanowires*

INTRODUCTION

Optical manipulation using light-induced forces has become an indispensable technique in many disciplines, ranging from mechanics, biology, and nanotechnology to quantum physics. As a counterintuitive phenomenon, the optical pulling force has recently received wide attention in the community.[1−7] Compared to the optical scattering force that always pushes objects away from the light source,[8−14] the optical pulling force can transport objects toward the source, providing additional degrees of freedom in optical manipulation. On the basis of the conservation law of linear momentum, the optical pulling force implies an increase in optical linear momentum along the forward direction. Therefore, to generate optical pulling forces, researchers have used various methods to enhance the forward linear momentum of light by engineering light−matter interactions. Some examples include using structured sources,[15] modifying the shapes or properties of objects,[16−19] and changing the background materials.[20−26] Meanwhile, arbitrary optical manipulation (both optical pulling and pushing forces) of metallic objects, including metallic spheres, nanorods, and nanowires, has attracted intense interest because they support surface plasmon resonances to enhance optical forces.[27−32] In particular, metallic nanowires are considered to be a promising building block for next-generation optoelectronic nanodevices.[33,34] Therefore, the on-demand, all-optical manipulation of metallic nanowires is highly desirable and requires an efficient strategy to generate optical pulling and pushing forces on metallic nanowires. However, such a strategy is still lacking, especially with a practical platform and the simple illumination of a plane wave.

Very recently, the topology-momentum-induced optical pulling force has been proposed by Ding and co-workers.[26] By choosing suitable parameters of a photonic crystal, the authors achieve an isofrequency contour of concave shape, which provides an increment of forward linear momentum for the field scattered from an elliptical dielectric object embedded inside the photonic crystal. As a result, the objects can be manipulated by the induced optical pulling force under the illumination of a simple plane wave rather than structured light with sophisticated beam profiles. The robust optical pulling force acting on the dielectric elliptical objects manifests a very

Received: September 30, 2021
Revised: November 30, 2021
Published: December 13, 2021

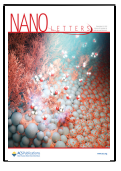

https://doi.org/10.1021/acs.nanolett.1c03772
Nano Lett. 2021, 21, 10431−10437

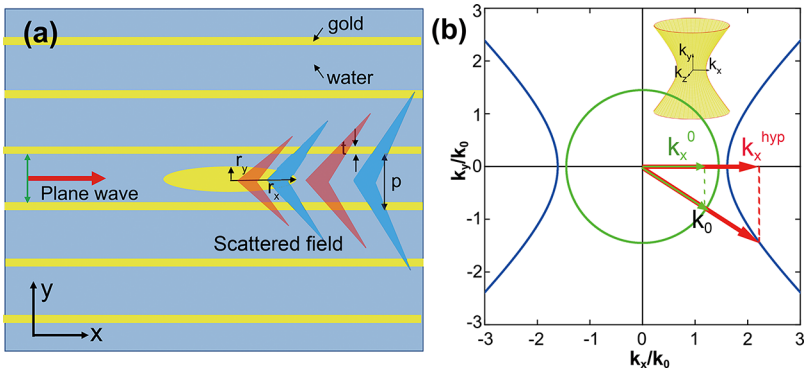

Figure 1. Schematical illustration of (a) an elliptical nanowire embedded in a gold−water multilayer HMM and (b) the mechanism of the optical pulling force induced by the concave isofrequency contour of an HMM. The inset in (b) shows the three-dimensional isofrequency contour.

interesting route for optical manipulation at the nanoscale. Nevertheless, further investigation is still needed. On the one hand, we need to substantially enhance the manipulation capabilities for various objects, considering their shape, size, and constituent materials. On the other hand, it is important to readily switch between the optical pulling force and the optical pushing force for arbitrary optical manipulation.

In this letter, we propose to use hyperbolic metamaterials (HMMs) to achieve robust optical pulling forces for gold nanowires. HMMs are extremely anisotropic materials that can be constructed by metal-dielectric multilayers or metallic nanowire arrays. Researchers have demonstrated super-resolution imaging,[35−38] anomalous cavity resonances,[39] negative refraction,[40−44] and topological transition based on HMMs.[45,46] One of the most unique properties of HMMs is the concave-shaped isofrequency over a broad wavelength range, which is expected to generate an optical pulling force due to the enhanced forward optical momentum.[47−49] It is worth mentioning that state-of-the-art manufacturing techniques demonstrate the possibility of fabricating such vertical HMMs.[50,51] In this work, we first consider a gold−water multilayer HMM and investigate the optical force acting on a gold elliptical particle inside the HMM.With the illumination of a transverse magnetic (TM) plane wave, we find that optical pulling forces can exist over a broad wavelength range. Since this configuration is difficult to use for experimental demonstration, we propose another theme in which a gold nanowire is placed above a gold−silica multilayer HMM. It is shown that under the oblique illumination of a plane wave with TM polarization, the gold nanowire also experiences a broadband optical pulling force. After carefully analyzing the near field, we find two factors collectively contributing to the optical pulling force. One is the topology of HMMs (i.e., the concave isofrequency contour), and the other is the excitation of directional surface plasmon polaritons (SPPs). A few papers have reported optical pulling forces in HMMs.[23,52,53] However, they either use the gradient field to generate the short-range optical pulling force[52,53] or trap only dielectric spheres without topology-momentum engineering.[23] Our approach could be leveraged to control other nanoscale objects such as quantum dots and biomolecules for many exciting applications.[54]

RESULTS AND DISCUSSION

We start with an HMM consisting of gold−water multilayers as shown in Figure 1a. The thickness of the gold layer is t, and the period of HMM is p, which is set as 60 nm. An elliptical gold nanowire is positioned inside the HMM. A plane wave with TM polarization (i.e., magnetic field parallel to the z axis) is incident from the left side. To study the influence of hyperbolic topology on the optical force acting on the elliptical gold nanowire, we define the filling ratio $f = t/p$, which represents the thickness ratio of the gold layer in one period. For an HMM made of metal−dielectric multilayers, the components of the effective permittivity parallel ($\varepsilon_{\parallel} = \varepsilon_y$) and perpendicular ($\varepsilon_{\perp} = \varepsilon_x = \varepsilon_z$) to the y axis are given by[47]

$$\begin{cases} \varepsilon_{\parallel} = \dfrac{\varepsilon_d \varepsilon_m}{\varepsilon_d f + \varepsilon_m (1-f)} \\ \varepsilon_{\perp} = \varepsilon_m f + \varepsilon_d (1-f) \end{cases} \tag{1}$$

Here, ε_d and ε_m denote the permittivity of the dielectric and the metal, respectively. In our model, $\varepsilon_d = 1.77$ is taken for water, and ε_m is taken from Johnson's experimental data for gold.[55]

Figure 1b illustrates the mechanism underlying the optical pulling force acting on the elliptical gold nanowire. The green circle represents the isofrequency contour of water, and the blue hyperbola is the isofrequency contour of an HMM. The oblique green arrow represents the electric field scattered from the nanowire when it is suspended in a pure water background. It has a smaller horizontal component ($k_x{}^0$) compared to that of the incident plane wave (i.e., k_0). However, when the nanowire is placed inside an HMM, the scattered electric field has an enhanced momentum due to the hyperbolic isofrequency contour of HMM (as indicated by the oblique red arrows). Obviously, this makes k_x^{hyp} greater than k_x^0 (horizontal red and green arrows, respectively) and hence causes increased momentum along the $+x$ axis. As a result, the increased momentum will induce an optical pulling force acting on the gold nanowire pointing, which is in the opposite direction to the incident plane wave. In the wavelength region of interest, the concave isofrequency contour of HMM exists when the magnetic field component of the incident light is along the z axis, i.e., transverse magnetic light. For transverse electric light of incidence, the HMM simply functions as a reflective metal film. In addition, we can use metallic nanowires embedded in a dielectric matrix to construct HMMs, which are expected to produce optical pulling forces based on the same principle.

To verify the above mechanism, we consider three different filling ratios, 0, 10, and 20%, corresponding to the thickness of the gold layer equal to 0, 6, and 12 nm, respectively. Apparently, the background material is pure water in the first case and HMM in the latter two. Figure 2a plots the effective

https://doi.org/10.1021/acs.nanolett.1c03772
Nano Lett. 2021, 21, 10431−10437

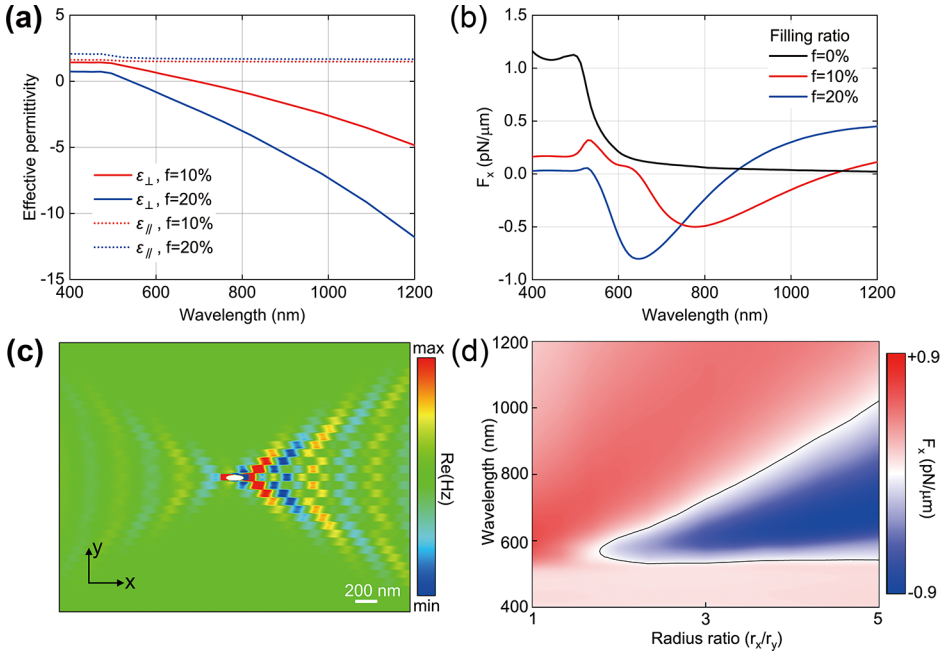

Figure 2. (a) Effective permittivity of gold−water multilayer HMM with filling ratios of 10 and 20%, respectively. (b) Optical forces acting on an elliptical gold nanowire with varied HMM background. (c) Scattered field of the elliptical gold nanowire at a wavelength of 650 nm. (d) Optical force acting on gold nanowires with different radius ratios. The black contour line corresponds to $F_x = 0$. The filling ratio of HMMs is 20%, and the incident power density is 10 mW·μm^{-2}.

permittivity of the two HMMs, which are calculated with eq 1. The dispersion relationship of TM polarized light propagating inside an anisotropic medium and within the $x-y$ plane is given by

$$\frac{k_x^2}{\varepsilon_y} + \frac{k_y^2}{\varepsilon_x} = \frac{k_x^2}{\varepsilon_\parallel} + \frac{k_y^2}{\varepsilon_\perp} = \frac{\omega^2}{c^2} \tag{2}$$

From eq 2, we can readily find that negative $\varepsilon_\perp$ and positive $\varepsilon_\parallel$ result in a hyperbolic isofrequency contour. This condition can be satisfied across a broad wavelength range according to Figure 2a.

We have performed full-wave simulations with commercial software Lumerical and applied the Maxwell stress tensor to calculate the optical force.[56−58] The time-averaged optical force is calculated by

$$\langle \mathbf{F} \rangle = \int_S \langle \mathbf{T} \rangle \cdot \mathbf{n} \, da \tag{3}$$

Here, $\mathbf{T}$ is the Maxwell stress tensor given by

$$\mathbf{T} = \varepsilon\varepsilon_0 \mathbf{EE} + \mu\mu_0 \mathbf{HH} - \frac{\mathbf{I}}{2}(\varepsilon\varepsilon_0 |\mathbf{E}|^2 + \mu\mu_0 |\mathbf{H}|^2) \tag{4}$$

In eqs 3 and 4, S is the surface enclosing the nanowire, $\mathbf{n}$ is the unit vector normal to the surface, da is the differential element of the surface, and $\mathbf{I}$ is the identity tensor. The power density of the incident plane wave is 10 mW·μm^{-2}. Figure 2b plots the x component of the optical force (F_x) acting on the elliptical gold nanowire. The radius along the x axis is r_x = 60 nm, and that along the y axis is r_y = 15 nm. Negative F_x corresponds to an optical pulling force that points toward the source. Obviously, when the filling ratios are 10 and 20%, we can achieve broadband optical pulling forces in the visible and near-infrared ranges. The onset wavelengths of the optical pulling force for a 10% filling ratio (red line) and a 20% filling ratio (blue line) are 640 and 550 nm, respectively, in good agreement with the prediction based on the effective permittivity in Figure 2a. For comparison, the pure-water background (black line, filling ratio f = 0%) always generates positive F_x, representing an optical pushing force. Figure 2c depicts the magnetic field scattered from the gold nanowire at a wavelength of 650 nm when the filling ratio is 20%. Under these conditions, the gold nanowire experiences the maximal optical pulling force. The scattered magnetic field shows a concave-shaped wavefront and is scattered off the x axis with large tilt angles. This result confirms our prediction of the mechanism of the topology-momentum-induced optical pulling force in HMMs. It is noted that negative F_x exists within a certain wavelength range (see blue and red lines in Figure 2b), although the concave isofrequency contour feature in HMMs is extremely broadband. To reveal the reason, we extract the same scattered magnetic field at a wavelength of 1000 nm for the case of f = 20% (Figure S1 in the Supporting Information), where the optical force is positive. The scattered magnetic field still shows a concave wavefront, whereas the backward scattering is also enhanced. Therefore, the competition of forward- and backward-scattered fields results in the limited bandwidth of the optical pulling force, which is still more than 300 nm. To investigate the dependency of optical forces on nanowire geometries, we tune the radius ratio (r_x/r_y) from 1 to 5 while maintaining r_y as a constant value of 15 nm. Figure 2d depicts the results of F_x versus radius ratio when the filling ratio of HMM is 20%. Optical pulling forces appear when the radius ratio is larger than 1.7 as a result of the significant off-axis scattered field. In addition, the bandwidth of the optical pulling force also increases as the radius ratio increases, which indicates that HMMs are a good platform for producing broadband optical pulling forces.

The above results demonstrate the principle and advantages of the HMM-assisted optical pulling force. However, it is not very practical to conduct experiments based on the

https://doi.org/10.1021/acs.nanolett.1c03772
Nano Lett. 2021, 21, 10431−10437

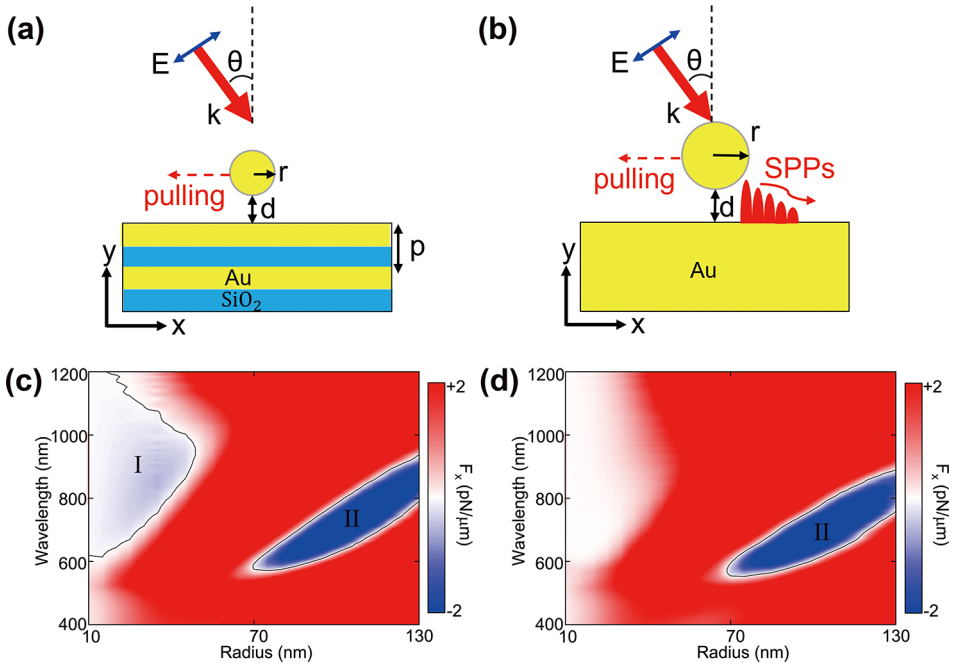

Figure 3. Schematic illustration of the simulation model in which a gold nanowire is placed 20 nm above (a) an HMM substrate and (b) a gold substrate. The corresponding optical forces versus nanowire radii are depicted in (c) and (d), respectively. The incident power density is 10 mW·μm^{-2}. The black contour lines correspond to F_x = 0.

configuration in Figure 1a. On the one hand, the gold nanowire is embedded in the gold−water multilayered HMMs. On the other hand, the typical gold nanowire has a radius ratio of 1, which cannot induce the optical pulling force according to the results in Figure 2d. Therefore, in the following, we propose an alternative yet more realistic platform to achieve the broadband HMM-assistant optical pulling force for typical gold nanowires. As schematically shown in Figure 3a, a gold nanowire is placed above an HMM substrate that consists of gold−SiO_2 multilayers. Considering the typical separation distance between a trapped object and a substrate due to the electrostatic interaction commonly used in similar computation,[14,59,60] we set a moderate separation of d = 20 nm in our simulation. A TM plane wave is input from the top surface with an oblique angle of incidence of θ = 25°. The gold nanowire has a radius r and infinite length. (Figure S2 in the Supporting Information presents the results for nanowires with finite lengths.) The HMM substrate has a period of p = 10 nm and a filling ratio of f = 50%. The ambient medium is water. Like the mechanism shown in Figure 1b, the increment of the forward linear momentum due to the concave-shaped isofrequency contour of HMMs induces a broadband optical pulling force. In addition, as plotted in Figure 3b, it is found that the excitation of directional SPPs also contributes to the optical pulling force, similar to that in previous work.[21−23]

As a proof-of-principle demonstration, we simulate the optical force acting on the gold nanowires with different radii. To verify the two aforementioned mechanisms, we compare the results of optical force acting on the gold nanowires with HMM and gold substrates, as illustrated in Figure 3a,b, respectively. In our simulations, the radius of gold nanowires is varied from 10 to 130 nm. Under the 25° illumination of a TM-polarized plane wave, F_x has negative values in two regions for both HMM and gold substrates, indicating the appearance of the optical pulling force, as outlined by black solid curves in Figure 3c. When the substrate is an HMM, a nanowire with a small radius (10 nm ≤ r ≤ 60 nm) experiences an optical pulling force, as marked by region I. Remarkably, the optical pulling force in this region has a considerable bandwidth, ranging from 620 to 1200 nm. In contrast, the optical pulling force acting on a larger nanowire (70 nm ≤ r ≤ 130 nm), which is marked by region II, has a relatively narrower bandwidth and a red shift with an increased radius. There is a noticeable difference (about 2−5-fold) in the magnitude of the optical pulling force between regions I and II. We think that the difference mainly comes from the size change of the gold nanowire. The gold nanowire in region I has a smaller radius than that in region II. A smaller nanowire scatters light less efficiently, and the excitation of SPPs is less pronounced in region I. As a result, region I is dominated by the topology-momentum-induced pulling force, while the force magnitude is very moderate. Figure 3d plots the simulated optical force when the substrate is gold. In this case, the optical pulling force exists only for large nanowires and follows a trend similar to that in region II in Figure 3c. Therefore, we can conclude that the optical pulling force in region II is not related to HMMs (Figure 1b). To further reveal the underlying mechanism, we detect the near-field distribution for both substrates. The electric fields show trends very similar to that in region II (Figure S3 in the Supporting Information). In addition, we have investigated the dependence of these two mechanisms on the separation d. The results are presented in section 4 in the Supporting Information. We choose two nanowires with radii equal to 25 and 100 nm. The influence of separation on the topology-momentum-induced (Figure S4a) and directional-SPPs-induced forces (Figure S4b) is quite distinct. The high sensitivity of the topology-momentum-induced optical pulling force can be attributed to the interaction between the gold nanowire and HMM. It implies that the optical pulling force in region II arises from the excitation of directional SPPs and the optical pulling force in region I comes from the topology-momentum increment in HMM.

https://doi.org/10.1021/acs.nanolett.1c03772
Nano Lett. 2021, 21, 10431−10437

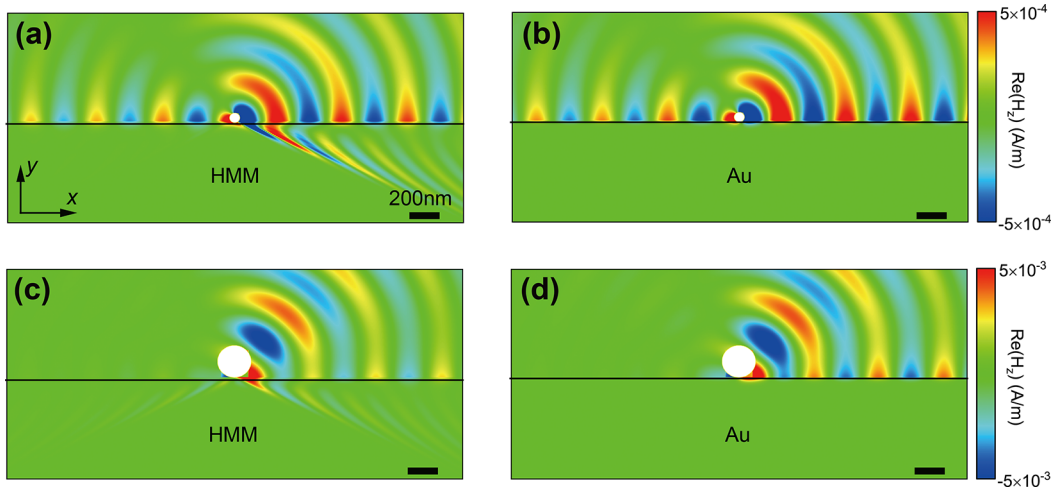

Figure 4. (a, b) Scattered H_z field when a gold nanowire (r = 25 nm) is above an HMM substrate and a gold substrate, respectively. (c, d) Scattered H_z field when a larger nanowire (r = 125 nm) is above an HMM substrate and a gold substrate, respectively. Black lines indicate the interface for the substrate and water. The wavelength is 800 nm for all cases, and the incident power density is 10 mW·μm^{-2}.

To better understand the two regions exhibiting an optical pulling force and the two mechanisms, we plot the scattered magnetic fields at a wavelength of 800 nm in Figure 4. Two different radii of gold nanowires are chosen: 25 nm (Figure 4a,b) and 125 nm (Figure 4c,d). Note that in Figure 4a,c the substrate is HMM, while for Figure 4b,d, the substrate is gold. The field distributions are distinctly different. As shown in Figure 4a,b, the SPPs propagate at the interface of the substrate and water along both the forward and backward directions. However, a large portion of the scattered field from the nanowire penetrates the HMM (Figure 4a) and propagates along the forward direction to form a concave shape. On the basis of the mechanism we demonstrated in Figure 1b, it generates a linear momentum enhancement along the $+x$ axis. As a result, the 25-nm-radius nanowire experiences an optical pulling force with an HMM substrate. For the nanowire in Figure 4b, although the generated forward SPPs appear to be stronger than the backward SPPs, the nanowire absorption balances the change in momentum. Without the HMM-induced momentum increment, the final force acting on the nanowire points in the $+x$ direction. The situations are totally different for the 125-nm-radius gold nanowires as shown in Figure 4c,d, where the unidirectional SPPs are always excited and propagate in the forward direction. Therefore, the 125-nm-radius gold nanowire experiences an optical pulling force with both substrates. We notice that Figure 4c still has a weak field penetrating the HMM substrate, which is expected to have a very small influence on the optical pulling force. To conclude, the field distributions are the direct evidence of the two mechanisms that induce optical pulling forces.

We have also explored the influence of the angle of incidence on the optical force. The angle of incidence is swept from 0 to 40° for a 25-nm-radius gold nanowire above an HMM substrate. The calculated optical force is plotted in Figure 5. Interestingly, the topology-momentum-induced optical pulling force acting on gold nanowires is not very sensitive to the angle of incidence, which is beneficial for experiments. When the angle of incidence is 0°, due to the lack of enhancement of forward linear momentum, no optical pulling forces exist. In the range from 1 to 20°, the optical pulling force has a large bandwidth from 600 to 1200 nm. However, when the angle of incidence is larger than 20°, the

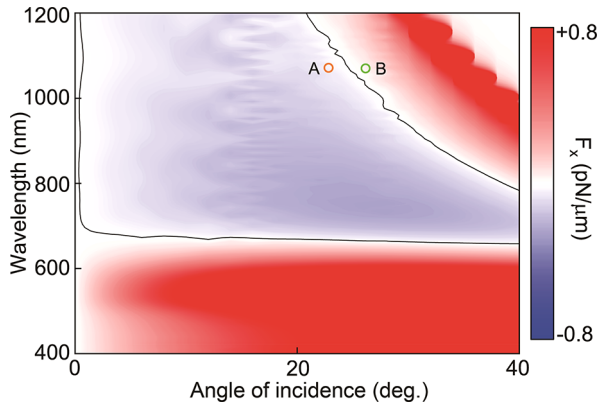

Figure 5. Angle dependence of the optical force acting on a 25-nm-radius gold nanowire above an HMM substrate. The incident power density is 10 mW·μm^{-2}.

bandwidth decreases. The reason is attributed to the dispersion of the isofrequency contour: the curvature of contours becomes larger (i.e., the contour is flatter) when the wavelength increases. The evolution of the isofrequency is shown in Figure S5 in the Supporting Information. As a result, the increment of forward linear momentum becomes less pronounced, and the momentum-topology-induced optical pulling force gradually disappears at longer wavelength. Nevertheless, the onset wavelength remains the same for the entire range of angles of incidence, corresponding to the emergence of the hyperbolic dispersion of the HMM substrate. In comparison, the onset wavelength of the SPP-induced optical pulling force will shift with the angle of incidence (Figure S6 in the Supporting Information). Overall, Figure 5 confirms that the optical pulling force induced by the topology-momentum increment is broadband and has a good tolerance for the angle of incidence. In addition, the results suggest a possible theme for achieving the controllable optical manipulation of a gold nanowire above the HMM substrate. Specifically, by controlling the angle of incidence, we can easily switch between pulling and pushing gold nanowires. For instance, in Figure 5, the angle of incidence at point A (the orange circle) is 22°, which possess a negative force of around −0.05 pN. On the contrary, point B (green circle) corresponds

https://doi.org/10.1021/acs.nanolett.1c03772
Nano Lett. 2021, 21, 10431−10437

to an angle of incidence of 26 degrees and a positive force of around 0.05 pN. It is worth mentioning that HMMs also enable optical pulling forces acting on dielectric nanowires (Figures S7 and S8 in the Supporting Information). To address the potential optothermal effect of HMMs, we have calculated the temperature distribution in our system. The results show that the temperature increase is less than 1 K in the region where optical pulling forces exist (Figure S9 in the Supporting Information), and it has a negligible effect on the optical force.

CONCLUSION

We have comprehensively studied the optical pulling force acting on gold nanowires in the presence of HMMs, either as a background material or a substrate. Importantly, we can achieve optical pulling forces over a broad wavelength range thanks to the unique concave isofrequency contour of HMMs. By comparing the simulated results of two substrates (i.e., HMMs and gold), we elucidate the two mechanisms that induce optical fulling forces. One arises from the strong forward-scattered fields in HMMs, and the other is due to the directional SPPs at the substrate−water interface. In addition, we study the influence of the angle of incidence on the optical forces. The results show that the topology-momentum-induced optical pulling force has a good tolerance for the angle of incidence. Furthermore, the arbitrary manipulation of gold nanowires can be achieved by simply changing the angle of incidence. We expect that our approach would pave the way for the arbitrary optical manipulation of various objects at different scales, and we find important applications in engineering, physics, biology, and other disciplines.

ASSOCIATED CONTENT

Supporting Information

The Supporting Information is available free of charge at https://pubs.acs.org/doi/10.1021/acs.nanolett.1c03772.

Additional data and discussions on the scattered field, electric field distribution, dependence of optical forces on the distance between the gold nanowire and substrate, angle dependence of optical forces in region II, optical forces acting on dielectric nanowires, and optothermal effect in HMMs (PDF)

AUTHOR INFORMATION

Corresponding Authors

Zheng-Gao Dong − *Physics Department, Southeast University, Nanjing 211189, China;* orcid.org/0000-0003-1655-0253; Email: zgdong@seu.edu.cn

Yongmin Liu − *Department of Mechanical and Industrial Engineering and Department of Electrical and Computer Engineering, Northeastern University, Boston, Massachusetts 02115, United States;* orcid.org/0000-0003-1084-6651; Email: y.liu@northeastern.edu

Authors

Renchao Jin − *Department of Mechanical and Industrial Engineering, Northeastern University, Boston, Massachusetts 02115, United States*

Yihao Xu − *Department of Mechanical and Industrial Engineering, Northeastern University, Boston, Massachusetts 02115, United States*

Complete contact information is available at: https://pubs.acs.org/10.1021/acs.nanolett.1c03772

Notes

The authors declare no competing financial interest.

ACKNOWLEDGMENTS

Y.L. acknowledges the financial support from the National Science Foundation (CBET-1931777 and DMR-1654192). Z.-G.D. acknowledges the financial support from the National Natural Science Foundation of China under grant number 11774053.

REFERENCES

(1) Chen, J.; Ng, J.; Lin, Z. F.; Chan, C. T. Optical Pulling Force. *Nat. Photonics* **2011**, *5*, 531−534.

(2) Sukhov, S.; Dogariu, A. On the Concept of "Tractor Beams". *Opt. Lett.* **2010**, *35*, 3847−3849.

(3) Brzobohaty, O.; Karásek, V.; Siler, M.; Chvátal, L.; Ci zmár, T.; Zemánek, P. Experimental Demonstration of Optical Transport, Sorting and Self-Arrangement Using a 'Tractor Beam'. *Nat. Photonics* **2013**, *7*, 123−127.

(4) Dogariu, A.; Sukhov, S.; Sáenz, J. J. Optically Induced 'Negative Forces'. *Nat. Photonics* **2013**, *7*, 24−27.

(5) Kajorndejnukul, V.; Ding, W. Q.; Sukhov, S.; Qiu, C. W.; Dogariu, A. Linear Momentum Increase and Negative Optical Forces at Dielectric Interface. *Nat. Photonics* **2013**, *7*, 787−790.

(6) Li, H.; Cao, Y.; Zhou, L.-M.; Xu, X.; Zhu, T.; Shi, Y.; Qiu, C.-W.; Ding, W. Optical Pulling Forces and Their Applications. *Adv. Opt. Photonics* **2020**, *12*, 288−366.

(7) Lu, J.; Yang, H.; Zhou, L.; Yang, Y.; Luo, S.; Li, Q.; Qiu, M. Light-Induced Pulling and Pushing by the Synergic Effect of Optical Force and Photophoretic Force. *Phys. Rev. Lett.* **2017**, *118*, 043601.

(8) Ashkin, A.; Dziedzic, J. M.; Bjorkholm, J. E.; Chu, S. Observation of a Single-Beam Gradient Force Optical Trap for Dielectric Particles. *Opt. Lett.* **1986**, *11*, 288−290.

(9) Grier, D. G. A Revolution in Optical Manipulation. *Nature* **2003**, *424*, 810−816.

(10) Juan, M. L.; Righini, M.; Quidant, R. Plasmon Nano-Optical Tweezers. *Nat. Photonics* **2011**, *5*, 349−356.

(11) Maragò, O. M.; Jones, P. H.; Gucciardi, P. G.; Volpe, G.; Ferrari, A. C. Optical Trapping and Manipulation of Nanostructures. *Nat. Nanotechnol.* **2013**, *8*, 807−819.

(12) Yan, Z.; Jureller, J. E.; Sweet, J.; Guffey, M. J.; Pelton, M.; Scherer, N. F. Three-Dimensional Optical Trapping and Manipulation of Single Silver Nanowires. *Nano Lett.* **2012**, *12*, 5155−5161.

(13) Yan, Z.; Pelton, M.; Vigderman, L.; Zubarev, E. R.; Scherer, N. F. Why Single-Beam Optical Tweezers Trap Gold Nanowires in Three Dimensions. *ACS Nano* **2013**, *7*, 8794−8800.

(14) Zhang, Y. Q.; Wang, J.; Shen, J. F.; Man, Z. S.; Shi, W.; Yuan, G. H.; Min, C. J.; Zhu, S. W.; Urbach, H. P.; Yuan, X.-C. Plasmonic Hybridization Induced Trapping and Manipulation of a Single Au Nanowire on a Metallic Surface. *Nano Lett.* **2014**, *14*, 6430−6436.

(15) Li, X.; Chen, J.; Lin, Z.; Ng, J. Optical Pulling at Macroscopic Distances. *Sci. Adv.* **2019**, *5*, No. eaau7814.

(16) Chen, H.; Liu, S.; Zi, J.; Lin, Z. Fano Resonance-Induced Negative Optical Scattering Force on Plasmonic Nanoparticles. *ACS Nano* **2015**, *9*, 1926−1935.

(17) Zhu, T.; Novitsky, A.; Cao, Y.; Mahdy, M. R. C.; Wang, L.; Sun, F.; Jiang, Z.; Ding, W. Mode Conversion Enables Optical Pulling Force in Photonic Crystal Waveguides. *Appl. Phys. Lett.* **2017**, *111*, 061105.

(18) Lee, E.; Huang, D.; Luo, E. Ballistic Supercavitating Nanoparticles Driven by Single Gaussian Beam Optical Pushing and Pulling Forces. *Nat. Commun.* **2020**, *11*, 2404.

(19) Lee, E.; Luo, T. Long-Distance Optical Pulling of Nanoparticle in a Low Index Cavity Using a Single Plane Wave. *Sci. Adv.* **2020**, *6*, No. eaaz3646.

(20) Intaraprasonk, V.; Fan, S. Optical Pulling Force and Conveyor Belt Effect in Resonator-Waveguide System. *Opt. Lett.* **2013**, *38*, 3264.

(21) Petrov, M. I.; Sukhov, S. V.; Bogdanov, A. A.; Shalin, A. S.; Dogariu, A. Surface Plasmon Polariton Assisted Optical Pulling Force. *Laser Photon. Rev.* **2016**, *10*, 116−122.
(22) Ivinskaya, A.; Petrov, M. I.; Bogdanov, A. A.; Shishkin, I.; Ginzburg, P.; Shalin, A. S. Plasmon-Assisted Optical Trapping and Antitrapping. *Light: Sci. Appl.* **2017**, *6*, No. e16258.
(23) Ivinskaya, A.; Kostina, N.; Proskurin, A.; Petrov, M. I.; Bogdanov, A. A.; Sukhov, S.; Krasavin, A. V.; Karabchevsky, A.; Shalin, A. S.; Ginzburg, P. Optomechanical Manipulation with Hyperbolic Metasurfaces. *ACS Photonics* **2018**, *5*, 4371−4377.
(24) Lin, L.; Kollipara, P. S.; Kotnala, A.; Jiang, T.; Liu, Y.; Peng, X.; Korgel, B. A.; Zheng, Y. Opto-Thermoelectric Pulling of Light-Absorbing Particles. *Light: Sci. Appl.* **2020**, *9*, 34.
(25) Zhu, T.; Cao, Y.; Wang, L.; Nie, Z.; Cao, T.; Sun, F.; Jiang, Z.; Nieto-Vesperinas, M.; Liu, Y.; Qiu, C.-W.; Ding, W. Q. Self-Induced Backaction Optical Pulling Force. *Phys. Rev. Lett.* **2018**, *120*, 123901.
(26) Li, H.; Cao, Y. Y.; Shi, B. Y.; Zhu, T. T.; Geng, Y.; Feng, R.; Wang, L.; Sun, F. K.; Shi, Y. Z.; Miri, M. A.; Nieto-Vesperinas, M.; Qiu, C.-W.; Ding, W. Q. Momentum-Topology-Induced Optical Pulling Force. *Phys. Rev. Lett.* **2020**, *124*, 143901.
(27) Barnes, W. L.; Dereux, A.; Ebbesen, T. W. Surface Plasmon Subwavelength Optics. *Nature* **2003**, *424*, 824−830.
(28) Dykman, L.; Khlebtsov, N. Gold Nanoparticles in Biomedical Applications: Recent Advances and Perspectives. *Chem. Soc. Rev.* **2012**, *41*, 2256−2282.
(29) Wang, X.; Li, Y.; Wang, H.; Fu, Q.; Peng, J.; Wang, Y.; Du, J.; Zhou, Y.; Zhan, L. Gold Nanorod-Based Localized Surface Plasmon Resonance Biosensor for Sensitive Detection of Hepatitis B Virus in Buffer, Blood Serum and Plasma. *Biosens. Bioelectron.* **2010**, *26*, 404−410.
(30) Linghu, S.; Gu, Z.; Lu, J.; Fang, W.; Yang, Z.; Yu, H.; Li, Z.; Zhu, R.; Peng, J.; Zhan, Q.; Zhuang, S.; Gu, M.; Gu, F. Plasmon-Driven Nanowire Actuators for On-Chip Manipulation. *Nat. Commun.* **2021**, *12*, 385.
(31) Tadesse, L. F.; Ho, C. S.; Chen, D. H.; Arami, H.; Banaei, N.; Gambhir, S. S.; Jeffrey, S. S.; Saleh, A. A. E.; Dionne, J. Plasmonic and Electrostatic Interactions Enable Uniformly Enhanced Liquid Bacterial Surface-Enhanced Raman Scattering (SERS). *Nano Lett.* **2020**, *20*, 7655−7661.
(32) Vadai, M.; Angell, D. K.; Hayee, F.; Sytwu, K.; Dionne, J. A. In Situ Observation of Plasmon-Controlled Photocatalytic Dehydrogenation of Individual Palladium Nanoparticles. *Nat. Commun.* **2018**, *9*, 4658.
(33) Lal, S.; Hafner, J. H.; Halas, N. J.; Link, S.; Nordlander, P. Noble Metal Nanowires: From Plasmon Waveguides to Passive and Active Devices. *Acc. Chem. Res.* **2012**, *45*, 1887−1895.
(34) Wei, H.; Xu, H. X. Nanowire-Based Plasmonic Waveguides and Devices for Integrated Nanophotonic Circuits. *Nanophotonics* **2012**, *1*, 155−169.
(35) Jacob, Z.; Alekseyev, L. V.; Narimanov, E. Optical Hyperlens: Far-Field Imaging Beyond the Diffraction Limit. *Opt. Express* **2006**, *14*, 8247−8256.
(36) Salandrino, A.; Engheta, N. Far-Field Subdiffraction Optical Microscopy Using Metamaterial Crystals: Theory and Simulations. *Phys. Rev. B: Condens. Matter Mater. Phys.* **2006**, *74*, 75103.
(37) Liu, Z.; Lee, h.; Xiong, Y.; Sun, C.; Zhang, X. Far-Field Optical Hyperlens Magnifying Sub-Diffraction-Limited Objects. *Science* **2007**, *315*, 1686−1686.
(38) Rho, J.; Ye, Z.; Xiong, Y.; Yin, X.; Liu, Z.; Choi, H.; Bartal, G.; Zhang, X. Spherical Hyperlens for Two-Dimensional Imaging at Visible Frequencies. *Nat. Commun.* **2010**, *1*, 143.
(39) Yang, X.; Yao, J.; Rho, J.; Yin, X.; Zhang, X. Experimental Realization of Three-Dimensional Indefinite Cavities at the Nanoscale with Anomalous Scaling Laws. *Nat. Photonics* **2012**, *6*, 450−453.
(40) Liu, Y.; Bartal, G.; Zhang, X. All-Angle Negative Refraction and Imaging in a Bulk Medium Made of Metallic Nanowires in the Visible Region. *Opt. Express* **2008**, *16*, 15439−15448.
(41) Yao, J.; Liu, Z.; Liu, Y.; et al. Optical Negative Refraction in Bulk Metamaterials of Nanowires. *Science* **2008**, *321*, 930−930.
(42) Xu, T.; Agrawal, A.; Abashin, M.; Chau, K. J.; Lezec, H. J. All Angle Negative Refraction and Active Flat Lensing of Ultraviolet Light. *Nature* **2013**, *497*, 470−474.
(43) Liu, Y.; Zhang, X. Metasurfaces for Manipulating Surface Plasmons. *Appl. Phys. Lett.* **2013**, *103*, 141101.
(44) High, A. A.; Devlin, R. C.; Dibos, A.; Polking, M.; Wild, D. S.; Perczel, J.; de Leon, N. P.; Lukin, M. D.; Park, H. Visible-Frequency Hyperbolic Metasurface. *Nature* **2015**, *522*, 192−196.
(45) Krishnamoorthy, H. N. S.; Jacob, Z.; Narimanov, E.; Kretzschmar, I.; Menon, V. M. Topological Transitions in Metamaterials. *Science* **2012**, *336*, 205−209.
(46) Gomez-Diaz, J. S.; Tymchenko, M.; Alu, A. Hyperbolic Plasmons and Topological Transitions over Uniaxial Metasurfaces. *Phys. Rev. Lett.* **2015**, *114*, 233901.
(47) Poddubny, A.; Iorsh, I.; Belov, P.; Kivshar, Y. Hyperbolic Metamaterials. *Nat. Photonics* **2013**, *7*, 948−957.
(48) Ferrari, L.; Wu, C.; Lepage, D.; Zhang, X.; Liu, Z. Hyperbolic Metamaterials and Their Applications. *Prog. Quantum Electron.* **2015**, *40*, 1−40.
(49) Huo, P.; Zhang, S.; Liang, Y.; Lu, Y.; Xu, T. Hyperbolic Metamaterials and Metasurfaces: Fundamentals and Applications. *Adv. Opt. Mater.* **2019**, *7*, 1801616.
(50) Kim, M.; Lee, D.; Kim, T. H.; Yang, Y.; Park, H. J.; Rho, J. Observation of Enhanced Optical Spin Hall Effect in a Vertical Hyperbolic Metamaterial. *ACS Photonics* **2019**, *6*, 2530−2536.
(51) Cho, H.; Yang, Y.; Lee, D.; So, S.; Rho, J. Experimental Demonstration of Broadband Negative Refraction at Visible Frequencies by Critical Layer Thickness Analysis in a Vertical Hyperbolic Metamaterial. *Nanophotonics* **2021**, *10*, 3871−3877.
(52) Shalin, A. S.; Sukhov, S. V.; Bogdanov, A. A.; Belov, P. A.; Ginzburg, P. Optical Pulling Forces in Hyperbolic Metamaterials. *Phys. Rev. A: At., Mol., Opt. Phys.* **2015**, *91*, 063830.
(53) Bogdanov, A. A.; Shalin, A. S.; Ginzburg, P. Optical Forces in Nanorod Metamaterial. *Sci. Rep.* **2015**, *5*, 15846.
(54) Solomon, M. L.; Saleh, A. A. E.; Poulikakos, L. V.; Abendroth, J. M.; Tadesse, L. F.; Dionne, J. A. Nanophotonic Platforms for Chiral Sensing and Separation. *Acc. Chem. Res.* **2020**, *53*, 588−598.
(55) Johnson, P. B.; Christy, R. W. Optical-Constants of Noble-Metals. *Phys. Rev. B* **1972**, *6*, 4370−4379.
(56) Yang, X.; Liu, Y.; Oulton, R. F.; Yin, X.; Zhang, X. Optical Forces in Hybrid Plasmonic Waveguides. *Nano Lett.* **2011**, *11*, 321−328.
(57) Zhang, T.; Mahdy, M. R. C.; Liu, Y.; Teng, J. H.; Lim, C. T.; Wang, Z.; Qiu, C.-W. All-Optical Chirality-Sensitive Sorting via Reversible Lateral Forces in Interference Fields. *ACS Nano* **2017**, *11*, 4292−4300.
(58) Jin, R. C.; Li, J. Q.; Li, L.; Dong, Z. G.; Liu, Y. Dual-Mode Subwavelength Trapping by Plasmonic Tweezers Based on V-Type Nanoantennas. *Opt. Lett.* **2019**, *44*, 319−322.
(59) Wang, K.; Schonbrun, E.; Crozier, K. B. Propulsion of Gold Nanoparticles with Surface Plasmon Polaritons: Evidence of Enhanced Optical Force from Near-Field Coupling between Gold Particle and Gold Film. *Nano Lett.* **2009**, *9*, 2623−2629.
(60) Min, C.; Shen, Z.; Shen, J.; Zhang, Y.; Fang, H.; Yuan, G.; Du, L.; Zhu, S.; Lei, T.; Yuan, X. Focused Plasmonic Trapping of Metallic Particles. *Nat. Commun.* **2013**, *4*, 2891.

https://doi.org/10.1021/acs.nanolett.1c03772
Nano Lett. 2021, 21, 10431−10437